Separation of Ground State and Transition State Effects in Intramolecular and Enzymatic Reactions. 2. A Theoretical Study of the Formation of Transition States in Cyclic Anhydride Formation

Felice C. Lightstone[1] and Thomas C. Bruice*

Contribution from the Department of Chemistry, University of California, Santa Barbara, California 93106

Abstract: *Ab initio* gas phase calculations at the RHF/6-31+G(d) level have been used to define the geometries of the transition states for the intramolecular displacement reactions with monophenyl esters of glutaric (**I**), succinic (**II**), and 3,6-endoxo-Δ^4-tetrahydrophthalic (**III**) acids to provide the corresponding anhydrides plus phenolate. As determined experimentally, the rate determining step was found to involve transition states in which phenoxide is departing. Intrinsic reaction coordinate (IRC) calculations from transition state toward reactant and product sides provided intramolecular ion−molecule complexes (IIMC) of **I** and **II** and the tetrahedral intermediate of **III** and the product ion−molecule complexes (IMC) of the phenoxide and anhydride of **I**, **II**, and **III**. Vibrational frequency calculations were performed for all stationary states. Single point calculations using an electron correlation method and different solvation methods were performed on optimized reactant side gas phase geometries. The transition states formed from **I**, **II**, and **III** are essentially identical in bond lengths (ester carbon to leaving phenoxide 1.77, 1.79, or 1.80 Å; carbonyl oxygen to ester carbon 1.20 or 1.21 Å; nucleophilic oxygen to ester carbon 1.44 or 1.43 Å; and α-carbon to ester carbon 1.52 or 1.53 Å) and angles (characterized by the attacking oxygen, ester carbon, and leaving oxygen 97.8°, 97.3°, 96.7°; attacking oxygen, ester carbon, and ester carbonyl oxygen 117.0°, 117.4°, 113.7°). Transition state stabilization as a result of restricting low frequency vibrations is determined by comparing the frequencies of the IIMC (and tetrahedral intermediate) to the corresponding TS. The total number of frequencies does not change in going from the IIMC (or TI) to the TS for each ester. For those frequencies lower than 1000 cm^{-1}, the number of frequencies remains constant. On comparing the ratio between the number of frequencies below 1000 cm^{-1} and the total number of frequencies in the transition states formed from **I**, **II**, and **III**, we find 0.49, 0.51, and 0.55, respectively. By the criteria of superimposable TS structures and lack of evidence for frequency changes in the TS in the direction of increasing rate, we conclude that the rate ratios of ∼230-fold in comparing **I/II** and **II/III** reside in ground state phenomena. This conclusion is supported by the geometries of IIMC and TS structures. Gas phase reaction coordinates and derived enthalpy and entropy values are provided and discussed. Conversion of ground state intramolecular anion ester complexes (IIMC) of esters **I** and **II** to their respective TSs involves a decrease in computed $\Delta H^{\ddagger}$ while $\Delta S^{\ddagger}$ remains invariant. In a previous investigation, the formation of ground state conformations (NACs) of geometry that allows entrance to the IIMC and then TS was found to be related to $\Delta H°$ rather than $\Delta S°$. The importance of these findings to a general concept of entropy driven kinetic processes is discussed.

Introduction

Studies of intramolecular reactions have been a subfield of organic chemistry. Derived concepts from the studies of the intramolecular anhydride formation by the monoesters of Table 1 have had a profound influence on the perception that the principal driving forces in enzymatic reactions are entropic. The kinetic importance of a decrease in entropy (translation) upon forming the ES complex is obvious. Further increase in rate to enhancements of 10^8 (as seen with the monoester of 3,6-endoxo-Δ^4-tetrahydrophthalate) have been attributed to a decrease in entropy by restriction of motion in the enzyme−substrate (ES) complex.[2] Results of this study will be discussed in terms of these concepts.

In a previous study[3] we employed a novel methodology for the computational analysis of intramolecular reactions. The case in point was the formation of five- and six-membered cyclic anhydrides (eq 1) from the monoesters of Table 1.[4] The procedure should be of general use when an acyclic compound
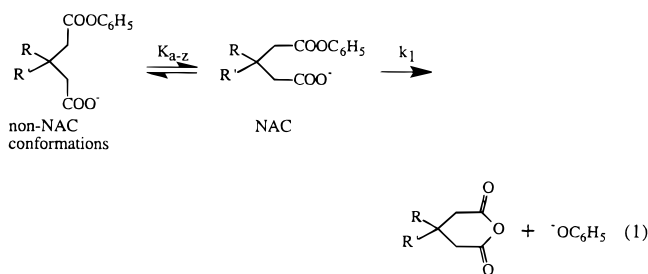
capable of existing in many conformations undergoes a reaction in which two reacting groups or atoms must approach each other in a particular geometry (**N**ear **A**ttack **C**onformation, NAC) in order to react. The first step is to define the geometry of the

---

[⊗] Abstract published in *Advance ACS Abstracts,* September 15, 1997.
(1) Contribution in partial satisfaction of the Ph.D. degree in chemistry.
(2) Page, M. I.; Jencks, W. P. *Proc. Natl. Acad. Sci. U.S.A.* **1971**, *68*, 1678.
(3) Lightstone, F. C.; Bruice, T. C. *J. Am. Chem. Soc.* **1996**, *118*, 2595.
(4) Pandit, K. P.; Bruice, T. C. *J. Am. Chem. Soc.* **1960**, *82*, 3386.

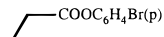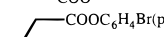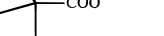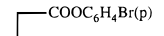**Table 1.** List of the Monophenyl Esters Used and Their Relative Rate Constants
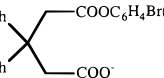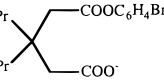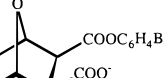
	k_{rel}
CH_3COO^- + $CH_3COOC_6H_5Br(p)$	1.0
I (COOC_6H_4Br(p) / COO^-)	1×10^3 M
(dimethyl, COOC_6H_4Br(p) / COO^-)	$\sim3.6 \times 10^3$ M
Et, Et (COOC_6H_4Br(p) / COO^-)	1.8×10^5 M
II (cyclopropane COOC_6H_4Br(p) / COO^-)	2.3×10^5 M
Ph, Ph (COOC_6H_4Br(p) / COO^-)	2.7×10^5 M
i-Pr, i-Pr (COOC_6H_4Br(p) / COO^-)	1.3×10^6 M
III (bicyclic O, COOC_6H_4Br(p) / COO^-)	$\sim8 \times 10^7$ M

Chart 1

NAC. For cyclic anhydride formation with the monoesters of Table 1, the geometry of the NAC was determined to be (*vide infra*) as shown in Chart 1.[3] The NAC is a genuine ground state conformation with reaction centers at $\sim$3 Å separation, such that bond making and breaking have not been initiated. Once the NAC has been defined, the problem can be viewed as consisting of two parts: (i) identifying ground state conformational equilibria and the formation of the NAC (by stochastic search combined with molecular mechanics) and (ii) locating the transition state in the conversion of the NAC to a product (using quantum mechanics). We feel that this approach is quite sensible since molecular mechanics is designed to deal with ground state energies. Without heroic measures, *ab initio* methods alone cannot be used to provide a useful analysis when the ground state consists of many stable conformations. This feature has not been generally recognized.

The molecular mechanical energetics of the formation of NACs for anhydride formation with the esters of Table 1 was the subject of our previous study.[3] In this report, we describe our *ab initio* quantum mechanical investigations of transition state structures, vibrational frequencies, and gas phase reaction trajectories for conversion of representative monoesters (of glutaric, succinic, and 3,6-endoxo-Δ^4-tetrahydrophthalic acids) to anhydrides. Before proceeding we would like to briefly review the procedures and findings of our previous study,[3] in so far as the three esters of the present study are concerned.
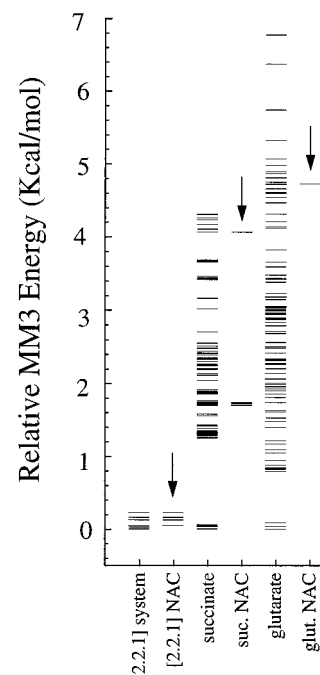
Figure 1. MM3 final energies of all local minimum conformations minus the energy of the most stable ground state conformation. The arrows point to the columns of the relative MM3 final energies of conformers that meet the near attack conformation (NAC) criteria.

Assignable conformations of each monoester of Table 1 were identified by first creating, as many as, 10 000 to 40 000 spatial isomers (as required to identify NAC structures), using Saunders stochastic search[5,6] method through MM3(92)[7] and discarding duplicates and those structures containing imaginary frequencies. The remaining structures were then individually energy minimized. In this manner, we obtained, for each monoester, a collection of the various conformations. Also obtained were the energies and thermodynamic parameters ($G°$, $H°$, and $S°$) for each of the various conformations. The Near Attack Conformations (NACs) could then be identified (Chart 1). Using the energies of the conformations and the Boltzmann equation, we calculated the mole fraction of conformations present as NACs for each ester (P). Figure 1 provides the energy distribution of the conformers of the three monoesters of concern in this study. Figure 2 is a plot of the log of the mole fraction of conformers (P) for the three esters present as NACs vs the log of the relative rate constants (k_r) for anhydride formation. One can conclude, from the slope (1.17) of the plot of log P vs log k_r that there is a direct relationship between the fraction of conformations present as NACs and $\Delta G^\ddagger$. In the inset, the values of P for these esters are related to the change in $\Delta H°$ on NAC formation rather than change in $T\Delta S°$ (Figure 2).

Materials and Methods

To simplify and reduce computational time, monophenyl esters, corresponding to the mono-*p*-bromophenyl esters employed in the kinetic studies, were used in all the calculations. These monophenyl esters are of glutarate (**I**), succinate (**II**), and 3,6-endoxo-Δ^4-tetrahydrophthalate (**III**) (Chart 2). The semiempirical AM1[8] calculations were performed using the AMPAC

(5) Saunders, M. *J. Am. Chem. Soc.* **1987**, *109*, 3150.
(6) Saunders, M. *J. Comput. Chem.* **1989**, *10*, 203.
(7) Allinger, N. L.; Zhu, Z.-Q. S.; Chen, K. *J. Am. Chem. Soc.* **1992**, *114*, 6120.
(8) Dewar, M. J. S.; Zoebisch, E. G.; Healy, E. F.; Stewart, J. J. P. *J. Am. Chem. Soc.* **1985**, *107*, 3902.
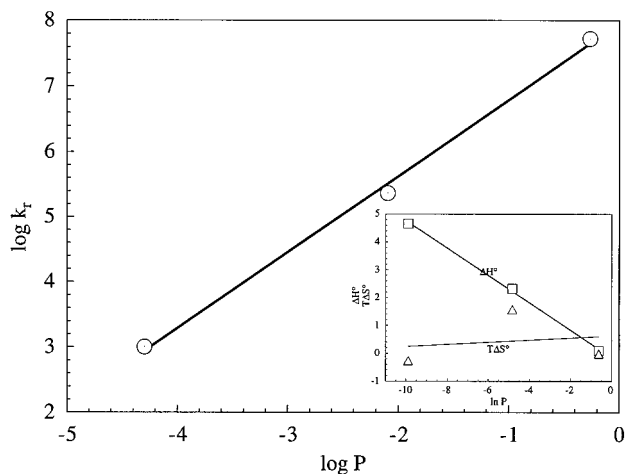
Figure 2. Plot of the log of the relative rate constants (k_r) for anhydride formation from esters **I**, **II**, and **III** vs the log of the mole fraction (**P**) of NAC formation. (For simplicity in determining **P**, computations of the distribution and stabilities of conformers were carried out with monophenyl esters, corresponding to the mono-*p*-bromophenyl esters used in the kinetic studies.) Inset: Plots of the MM3 enthalpy and MM3 entropy, assuming an equilibrium between the favored ground state conformation and the lowest energy near attack conformation (NAC) vs the log of the probability of being in a NAC.

Chart 2

glutarate

succinate

3,6-endoxo-Δ⁴-tetrahydrophthalate
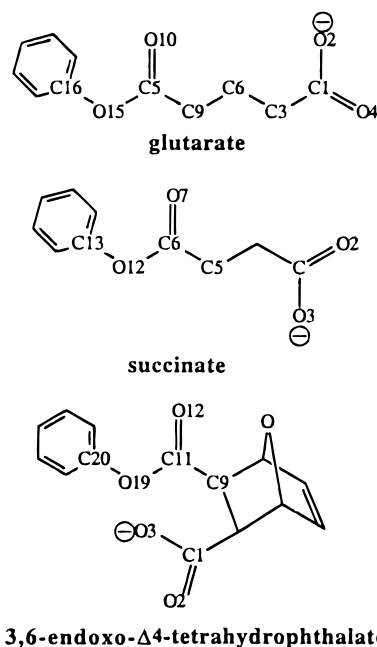
package.[9] The *ab initio* molecular orbital calculations were performed using Gaussian 92[10] or Gaussian 94[11] or SPARTAN[12]

(9) *Ampac 5.0*; Semichem, Shawnee, KS, 1994.

(10) Frisch, M. J.; Trucks, G. W.; Head-Gordon, M.; Gill, P. M. W.; Wong, M. W.; Foresman, J. B.; Johnson, B. G.; Schlegel, H. B.; Robb, M. A.; Replogle, E. S.; Gomperts, R.; Andres, J. L.; Raghavachari, K.; Binkley, J. S.; Gonzalez, C.; Martin, R. L.; Fox, D. J.; Defrees, D. J.; Baker, J.; Stewart, J. J. P.; Pople, J. A. *Gaussian 92*; Gaussian, Inc.: Pittsburgh, PA, 1992.

(11) Frisch, M. J.; Trucks, G. W.; Schlegel, H. B.; Gill, P. M. W.; Johnson, B. G.; Robb, M. A.; Cheeseman, J. R.; Keith, T. A.; Petersson, G. A.; Montgomery, J. A.; Raghavachari, K.; Al-Laham, M. A.; Zakrzewski, V. G.; Ortiz, J. V.; Foresman, J. B.; Cioslowski, J.; Stefanov, B. B.; Nanayakkara, A.; Challacombe, M.; Peng, C. Y.; Ayala, P. Y.; Chen, W.; Wong, M. W.; Andres, J. L.; Replogle, E. S.; Gomperts, R.; Martin, R. L.; Fox, D. J.; Binkley, J. S.; Defrees, D. J.; Baker, J.; Stewart, J. P.; Head-Gordon, M.; Gonzalez, C.; Pople, J. A. *Gaussian 94*; Gaussian, Inc.: Pittsburgh, PA, 1995.

(12) *Spartan 4.0*; Wavefunction, Inc., Irvine, CA, 1995.

at the restricted Hartree−Fock (RHF) level of theory. All optimized structures are in the gas phase. Initial geometries for the *ab initio* calculations were found using AM1 by creating reaction coordinates from the near attack conformation (NAC) to the tetrahedral intermediate and reaction coordinates from the tetrahedral intermediate to the leaving of the phenoxide group. Molecular geometries were reoptimized by using the energy gradient method at the RHF/6-31+G(d) level of theory. Transition states were located at the RHF/6-31+G(d) level. Intrinsic Reaction Coordinate (IRC) calculations were performed at the RHF/6-31+G(d) level of theory toward the reactant and product sides. Reactant and product side structures were optimized. The anhydride products were optimized with C_s symmetry, and the phenoxide was optimized with C_{2v} symmetry. All stationary points were characterized by vibrational frequency calculations, and all frequencies were corrected by 0.89.[13] Thermodynamic properties were calculated using the HF/6-31+G(d) calculated frequencies at 298.15 K. Single point calculations using various solvation methods, with the dielectric constant of water ($\epsilon = 78.3$), and density functional theory (RHF/6-31+G(d)/SCRF-SCIPCM, B3LYP/6-31+G(d), B3LYP/6-31+G(d)/SCRF-SCIPCM, AM1/SM2.1) were performed on reactant side gas phase RHF/6-31+G(d) geometries for the reaction of **I**, **II**, and **III**.

Results

Computational efforts in this study have been directed toward the elucidation of the transition states for the intramolecular reactions of the monophenyl esters of glutarate (**I**), succinate (**II**), and 3,6-endoxo-Δ⁴-tetrahydrophthate (**III**) esters to form the corresponding anhydride (eq 1). By intrinsic reaction coordinate (IRC) calculations, the structures preceding the transition state {intramolecular ion−molecule complex (IIMC) and tetrahedral intermediate (TI)} and following the transition state (ion−molecule complex, IMC) are also determined. All products, and extended structures for glutarate and succinate monoesters, are also calculated. In all reactions, the rate determining step was found to involve transition states in which phenoxide is departing. This is in agreement with previously published experimental findings.[4]

Structures Formed from Glutarate Monoester (I). The first step was to locate a transition state. From the AM1 reaction coordinate calculations, the rate determining transition state (TS) is formed from a tetrahedral intermediate. Starting with the AM1 TS, *ab initio* molecular orbital theory at the RHF/6-31+G-(d) level yielded one transition state with one imaginary frequency of 296.3*i* cm⁻¹ (Chart 3). The energy and selected geometrical parameters of this transition state are listed in Table 2. This particular intramolecular reaction can only have two possible transition state conformations: (i) the center methylene (C6) is puckered toward the ester carbonyl or (ii) the center methylene (C6) is puckered away from the ester carbonyl. Only the transition state characterized by the center methylene (C6) puckering toward the ester carbonyl was found. Also, the transition state is early insofar as departure of the leaving phenoxide oxygen (O15) to C5 is 1.77 Å (Chart 3). *Ab initio* optimization of the AM1 tetrahedral intermediate at the RHF/6-31+G(d) level resulted in the lengthening of the bond between attacking carboxylate oxygen and carbon (O2−C5) such that the tetrahedral intermediate does not exist as a minimum on the *ab initio* energy surface. IRC calculations from the transition state to the reactant side also did not find a tetrahedral intermediate which corresponded to the single imaginary

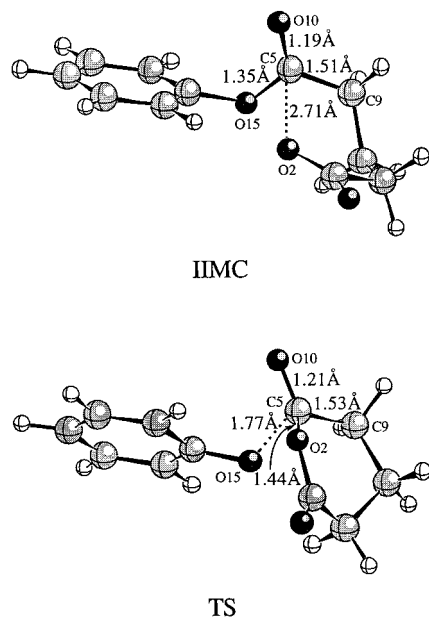(13) DeFrees, D. J.; McLean, A. D. *J. Chem. Phys* **1985**, *82*, 333.

Chart 3

IIMC

TS

Table 2. Total Energies and Selected Bond Lengths, Angles, and Dihedrals for the Transition State (TS), IIMC, and Product Side Ion−Molecule Complex (IMC) Formed from the Glutarate Monophenyl Ester

	TS	IIMC	IMC
RHF energy (Hartrees)	−722.46225	−722.49565	−722.48865
O(2)−C(1)	1.320	1.242	1.361
C(5)−O(2)	1.440	2.708	1.361
C(9)−C(5)	1.529	1.508	1.502
O(10)−C(5)	1.211	1.187	1.184
O(15)−C(5)	1.765	1.346	4.056
∠C(9)−C(5)−O(2)	112.44	86.49	117.65
∠O(10)−C(5)−O(2)	113.73	102.56	117.24
∠C(15)−C(5)−O(2)	97.76	88.24	93.42
∠O(10)− C(5)−C(9)	120.35	124.78	125.11
∠O(10)− C(5)−C(15)	112.06	122.71	133.86
∠O(15)−C(5)−C(9)	96.70	111.79	41.71
τ[C(16)−O(15)−C(5)−O(10)]	−22.33	−16.23	−13.57

Table 3. Total Energies for the Phenoxide, Glutarate, Succinate, and 3,6-Endoxo-Δ^4-tetrahydrophthalate ([2.2.1] System) Anhydrides and the Extended Structures of Glutarate and Succinate[a]

compound	RHF energy (Hartrees)
phenoxide	−304.99536
glutarate anhydride	−417.46115
succinate anhydride	−378.43012
[2.2.1] system anhydride	−605.88757
extended glutarate	−722.49252
extended succinate	−683.46113

[a] All energies in Hartrees.

frequency of the transition state. Observations of the geometry changes along the calculated IRC show the attack of carboxylate oxygen (O2) on carbon (C5) to be concerted with departure of the phenolate leaving group (O15). The optimized IIMC ground state is characterized by a short attack (C5···O2) distance of 2.71 Å (Chart 3) and by the center methylene carbon (C6) puckering away from the ester carbonyl. The IIMC energy and selected geometrical features are listed in Table 2.

When calculated separately, the anhydride and the phenoxide, final products, are higher in energy than the transition state (Table 3). IRC calculations from the transition state to the product side yielded an ion−molecule complex (IMC) of anhydride and phenoxide that is lower in energy compared to
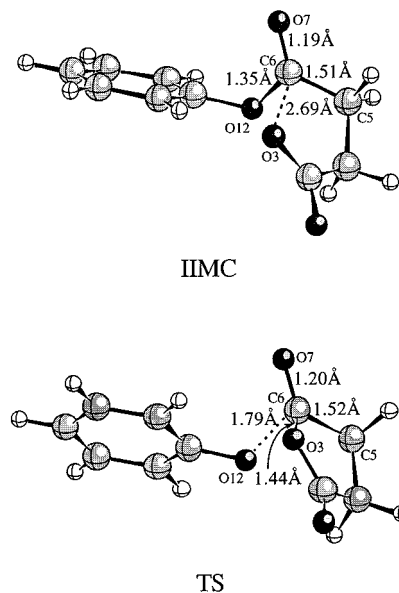
Chart 4

IIMC

TS

Table 4. Total Energies and Selected Bond Lengths, Angles, and Dihedrals for the Transition State (TS), IIMC, and Product Side Ion−Molecule Complex (IMC) Formed from the Succinate Monophenyl Ester

	TS	IIMC	IMC
RHF energy (Hartrees)	−683.43692	−683.46504	−683.45543
O(3)−C(1)	1.317	1.242	1.354
C(6)−O(3)	1.440	2.690	1.354
C(6)−C(5)	1.523	1.506	1.509
O(7)−C(6)	1.205	1.188	1.180
O(12)−C(6)	1.793	1.349	3.023
∠C(5)−C(6)−O(3)	104.54	75.79	109.86
∠O(7)−C(6)−O(3)	116.98	108.94	121.42
∠O(7)−C(6)−C(5)	125.79	125.36	128.58
∠O(12)−C(6)−O(3)	97.27	89.67	82.30
∠O(12)−C(6)−C(5)	93.98	111.99	68.23
∠O(12)−C(6)−O(7)	112.50	122.25	119.91
τ[C(13)−O(12)−C(6)−O(7)]	30.44	20.51	34.33

either the transition state or the final products. The energy and selected bond lengths and angles of the IMC are also listed in Table 2.

Structures Formed from Succinate Monoester (II). The *ab initio* transition state structure (Chart 4) at the RHF/6-31+G-(d) level of theory was found starting from the AM1 derived TS structure. Selected geometrical features of the transition state are listed in Table 4. This structure is characterized by one imaginary frequency at 293.6*i* cm^{-1}. The bond length of the breaking bond (O12−C6) is 1.79 Å. This was the only transition state found. Similar to the AM1 calculations with **I**, the AM1 calculations of **II** located a tetrahedral intermediate (TI). Starting with the AM1 TI structure, *ab initio* optimizations at the RHF/6-31+G(d) level did not yield a tetrahedral intermediate. Further efforts to locate a tetrahedral intermediate, starting from the five-membered ring geometry of the TI generated from **III**, failed. An IRC calculation from the transition state to the reactant side also did not result in a tetrahedral intermediate between TS and IIMC. The IIMC was optimized with an attacking oxygen (O3) to carbonyl carbon (C6) distance of 2.69 Å (Chart 4). Selected bond lengths, angles, and dihedral angles are listed in Table 4. IRC calculations were also performed toward the product side yielding an ion−molecule complex of anhydride and phenolate anion (IMC) that is lower in energy than the transition state and the products. In addition to the selected IMC geometrical parameters, Table 4 lists all the energies for the optimized structures of the
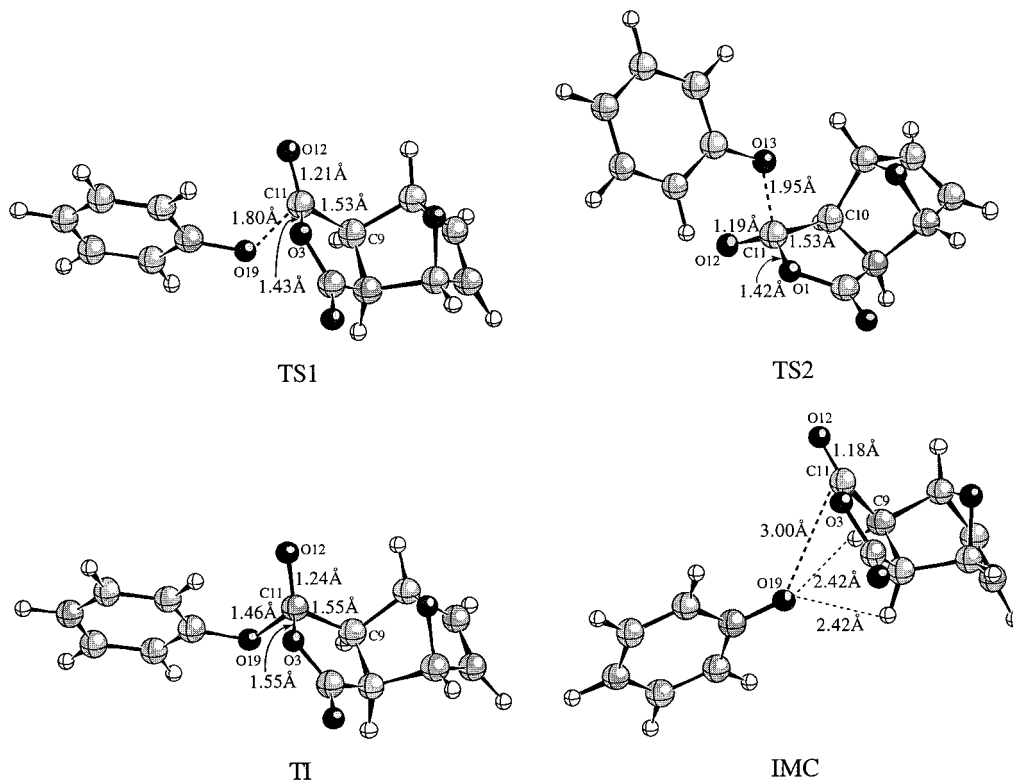
Chart 5

TS1

TS2

TI

IMC

Table 5. Total Energies and Selected Bond Lengths, Angles, and Dihedrals for the Transition State (TS), Tetrahedral Intermediate (TI), and Product Side Ion−Molecule Complex (IMC) Formed from the 3,6-Endoxo-Δ^4-tetrahydrophthalate Monophenyl Ester

	TS	TI	IMC
RHF energy (Hartrees)	−910.89306	−910.89989	−910.91324
O(3)−C(1)	1.315	1.291	1.352
C(11)−O(3)	1.430	1.550	1.352
C(11)−C(9)	1.527	1.545	1.511
O(12)−C(11)	1.206	1.239	1.180
O(19)−C(11)	1.796	1.459	2.999
∠C(9)−C(11)−O(3)	106.28	101.56	110.20
∠O(12)−C(11)−O(3)	117.36	112.70	121.70
∠O(19)−C(11)−O(3)	96.68	100.53	82.17
∠O(12)−C(11)−C(9)	124.83	120.30	127.98
∠O(19)−C(11)−C(9)	92.72	102.42	68.23
∠O(19)−C(11)−O(12)	112.80	116.54	119.89
τ[C(20)−O(19)−C(11)−O(12)]	−34.02	−41.70	−34.89

succinate monophenyl ester, the IIMC, the transition state, and the product IMC. The final products (anhydride and phenoxide) are higher in energy than the transition state, and their energies are listed in Table 3.

Structures Formed from 3,6-Endoxo-Δ^4-tetrahydrophthalate Monoester (III). Two transition states each with one imaginary frequency at 279.0i and 233.8i cm^{-1}, respectively, were found at the RHF/6-31+G(d) level of theory (Chart 5). Structure TS1 is lower in energy than TS2 by 8.7 kcal/mol. Because TS2 has a significantly higher energy than TS1, no further calculations were derived from TS2 (e.g., IRC calculations). TS1 is characterized by a bond length (C11−O19) of 1.80 Å (Chart 5) for departure of phenoxide. The energy and selected geometrical features of TS1 are listed in Table 5. The AM1 calculations with **III** optimized to a tetrahedral intermediate. Because of failures to optimize an *ab initio* level tetrahedral intermediate directly from the AM1 structure for **I** and **II**, no direct attempts to optimize the tetrahedral intermediate at the *ab initio* levels were made with **III**. However, IRC calculations from the transition state to the reactant side did result in a

tetrahedral intermediate. This intermediate is identified by the newly formed carboxyl to carbon bond (O3−C11) of 1.55 Å and the carbon to phenoxide bond (C11−O19) of 1.46 Å (Chart 5). Being characterized by only real frequencies, this intermediate is a genuine energy minimum. The energy and selected geometrical parameters of the tetrahedral intermediate are listed in Table 5. IRC calculations were also performed toward the product side to yield an ion−molecule complex (IMC) which is lower in energy than the transition state and the products. The IMC's energy and selected bond lengths and angles are listed in Table 5.

Geometries of Extended Ground State Structures of Esters I and II. AM1 optimized structures for a fully extended glutarate and a fully extended succinate esters, both in the staggered position, were used as starting structures for *ab initio* molecular orbital calculations. Each optimized structure at the HF/6-31+G(d) level was characterized by only real frequencies and positive eigenvalues (Chart 6). Their energies are listed in Table 3. The extended structure of **I** has a higher energy than its IIMC by 2.0 kcal/mol, and the extended structure of **II** has a higher energy than its IIMC by 2.5 kcal/mol. All attempts to optimize a relaxed structure of the 3,6-endoxo-Δ^4-tetrahydrophthalate ester resulted in a tetrahedral intermediate (Chart 5).

Vibrational Frequencies. Frequency calculations were performed for all stationary points. All frequencies were uniformly scaled by 0.89 because calculated *ab initio* frequencies are generally about 10 −15% larger than the experimental values.[13,14] For the transition states (TS) and the intramolecular ion−molecule complex (IIMC), the frequencies are shown in Figure 3 with only one imaginary frequency for each TS. The number of frequencies below 1000 cm^{-1} for the IIMC and the TS structures for the reactions of **I**, **II**, and **III** are in Table 6. The ratios between the low frequencies and the total frequencies for both IIMC and TS are also in Table 6.

(14) Hehre, W. J.; Radom, L.; Schleyer, P. v. R.; Pople, J. A. *Ab Initio Molecular Orbital Theory*; Wiley: New York, New York, 1986.

9108   *J. Am. Chem. Soc., Vol. 119, No. 39, 1997*

Lightstone and Bruice

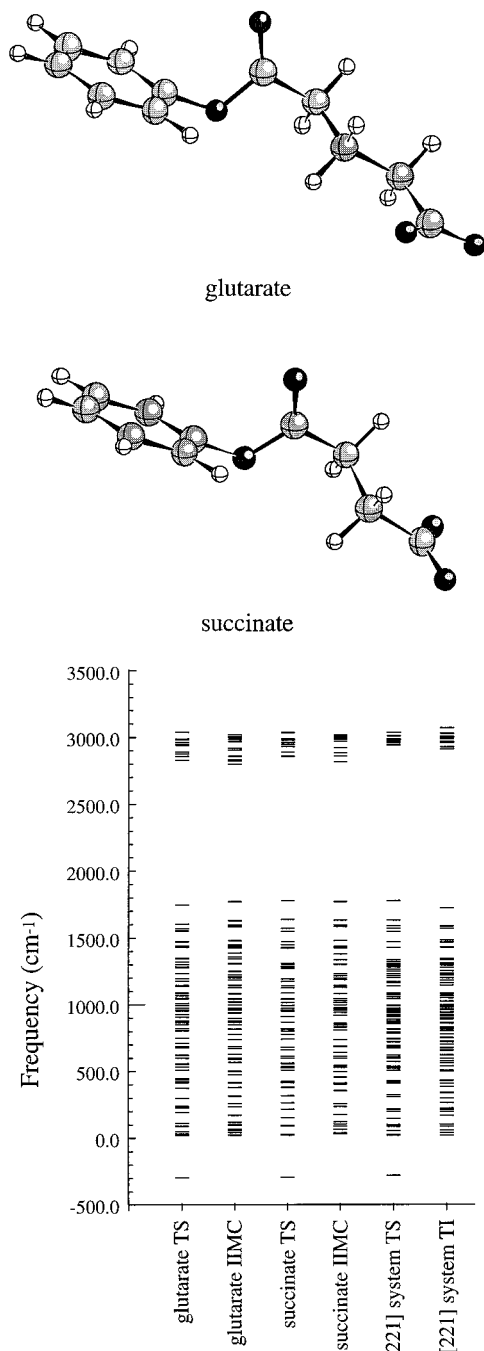**Chart 6**

glutarate

succinate

Figure 3. Plots of the frequencies for both intramolecular ion–molecule complex (IIMC) and transition state (TS) for the glutarate, succinate, and 3,6-endoxo-Δ^4-tetrahydrophthalate monophenyl ester reactions. As observed, the transition states have one imaginary frequency.

Solvation and Electron Correlation Calculations. Single point calculations with different solvation methods with a dielectric constant of water were performed on the optimized RHF/6-31+G(d) structures derived from **I**, **II**, and **III**. Only reactant side structures, including the TS, were chosen, and the resulting activation barriers are reported in Table 7. The HF solvation model resulted in larger barriers than the gas phase barriers, with the extended conformations for **I** and **II** being lower in energy than their respective IIMCs. For comparing the values from the B3LYP/SCRF-SCIPCM calculations, gas phase single point calculations were also performed with the B3LYP method. Like the RHF gas phase calculations, the B3LYP gas phase IIMCs for **I** and **II** are lower in energy than

Table 6. The Number of Frequencies for the IIMC and the TS for the Intramolecular Reactions of Glutarate (**I**), Succinate (**II**), and 3,6-Endoxo-Δ^4-tetrahydrophthalate (**III**) Monophenyl Esters
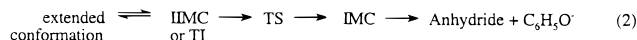
| | number of frequencies below 1000 cm^{-1} | | | Ratios | |
| | | | | IIMC | TS |
compound	IIMC or TI	TS	total	total	total
I	35	35	72	0.49	0.49
II	32	32	63	0.51	0.51
III	46[a]	46	84	0.55	0.55

[a] Ester **III** yields to a TI instead of an IIMC.

their respective extended structures. In the B3LYP/SCRF-SCIPCM solvation model, the calculations for the extended structures of **I** and **II** did not converge, and thus, their energies are not reported. Because the AM1/SM2.1 solvation model was parameterized to reproduce experimental hydration free energies, single point calculations were also performed with the AM1/SM2.1 method. For these calculations, the *ab initio* geometries were used for the calculations. The free energy of solvation from the AM1/SM2.1 calculations were then added to the gas phase HF/6-31+G(d) energies.

Discussion

Gas Phase Reaction Coordinate. Reaction coordinates play a role in the understanding of reaction mechanisms. Let us dissect the *ab initio* gas phase stationary points of the reaction coordinate for the monophenyl ester intramolecular reaction (eq 2). The structures of the extended conformations, intramolecular

$$\text{extended conformation} \rightleftharpoons \text{IIMC or TI} \longrightarrow \text{TS} \longrightarrow \text{IMC} \longrightarrow \text{Anhydride} + C_6H_5O^- \qquad (2)$$

ion–molecule complexes (IIMC) or tetrahedral intermediate (TI), and the transition state (TS) of the reaction for glutarate, succinate, and 3,6-endoxo-Δ^4-tetrahydrophthalate monophenyl esters are shown in Charts 3–6. Selected bond distances are also shown in these charts. The reaction coordinates for the reactions of **I** (a), **II** (b), and **III** (c) are shown in Figure 4. The activation energy in going from the intramolecular ion–molecule complex (IIMC) or tetrahedral intermediate (TI) to the TS decreases in going from reactions of **I** to **II** to **III**. For the reactions of **I** and **II**, the extended conformations are higher in energy than the IIMC but lower in energy than the TS. To place the gas phase reaction coordinates (Figure 4) in proper perspective, they may be compared to those for S_N2 attack of HO^- and CH_3COO^- on dichloroethane.[15] In the reaction of HO^- and dichloroethane, the reactants are higher in energy than the transition state. However, in the reaction of CH_3COO^- and dichloroethane, the reactants are slightly lower in energy than the transition state due to resonance stabilization of the negative charge in CH_3COO^-. Because of similar resonance stabilization, the extended ground state structures of **I** and **II** are substantially lower in energy than their respective TSs and only slightly higher than their intramolecular ion–molecule complexes (IIMCs). As for the product side, the ion–molecule complex (IMC) for the anhydrides from **I** and **II** are higher in energy than the IIMC, while the IMC for the formation of the anhydride from **III** is lower in energy than the TI. All final products are higher in energy than their respective transition states.

Structural Identity of TSs Formed from I, II, and III. The transition states in the formation of anhydrides from the monophenyl esters of glutaric (**I**), succinic (**II**), and 3,6-endoxo-Δ^4-tetrahydrophthalic (**III**) acids are essentially identical, as

(15) Maulitz, A. H.; Lightstone, F. C.; Zheng, Y.-J.; Bruice, T. C. *Proc. Natl. Acad. Sci. U.S.A.* **1997**, *94*, 6591.

Table 7. Activation Barriers to the TS Based on Solvation Single Point Calculations and Electron Correlation Single Point Calculations with the 6-31+G(d) Basis Set on the Optimized RHF/6-31+G(d) Structures

ester	process	HF/SCRF-SCIPCM (kcal/mol)	B3LYP (kcal/mol)	B3LYP/SCRF-SCIPCM (kcal/mol)	AM1/SM2.1 (kcal/mol)
I	extended conformation → TS	30.83	9.60	NA[a]	33.34
	IIMC → TS	27.62	11.65	17.67	33.78
II	extended conformation → TS	26.83	6.62	NA[a]	26.66
	IIMC → TS	26.16	8.56	15.32	29.69
III	TI → TS	6.72	1.92	3.81	5.84

[a] The data are not available because the single point calculations for the extended conformations did not converge.
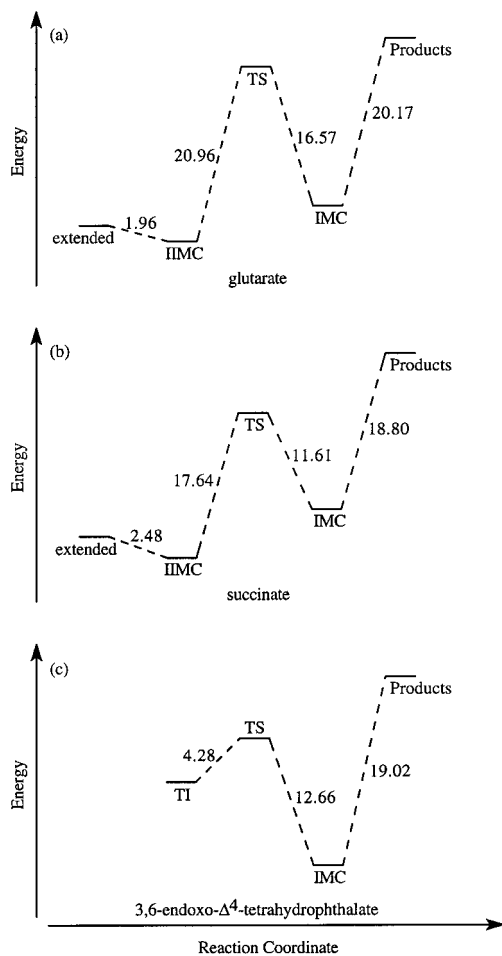

Figure 4. Gas phase RHF/6-31+G(d) reaction coordinate for the reactions of (a) glutarate monophenyl ester, (b) succinate monophenyl ester, and (c) 3,6-endoxo-Δ^4-tetrahydrophthalate monophenyl ester. All energies are energy differences (kcal/mol) between states.

Figure 5. An overlay of the transition states of anhydride formation of the monophenyl esters of glutaric, succinic, and 3,6-endoxo-Δ^4-tetrahydrophthalic acid. The black figure is the transition state of succinate; the middle gray figure is the transition state of 3,6-endoxo-Δ^4-tetrahydrophthalate; and the light gray figure is the transition state of glutarate. Where the ester moiety overlaps, the structure is shown in black as the succinate. The shown bond lengths are color coded with the figure.

shown in Figure 5. The bond length between ester carbon and leaving phenoxide are 1.77, 1.79, and 1.80 Å in the TS structures formed from **I**, **II** and **III**, respectively. The carbonyl oxygen–carbon bond lengths are 1.20 or 1.21 Å. The newly forming bond between the nucleophilic oxygen and the ester carbon have lengths of 1.44 or 1.43 Å, and the bond lengths between the α-carbon and the ester carbon are 1.52 or 1.53 Å. The bond angles for the transition states are also very similar. Comparing the angle characterized by the attacking oxygen, the ester carbon, and the leaving phenoxide oxygen, the TS for reaction **I** has an angle (O2–C5–O15) of 97.8°; for reaction **II**, an angle (O3–C6–O12) of 97.3°; and for reaction **III**, an angle (O3–C11–O19) of 96.7°. The angle comprised of the attacking oxygen, the ester carbon, and the ester carbonyl oxygen for the TS for reactions **II** (O3–C6–O7) and **III** (O3–C11–O12) are almost identical, 117.0° and 117.4°, respectively. This angle for the
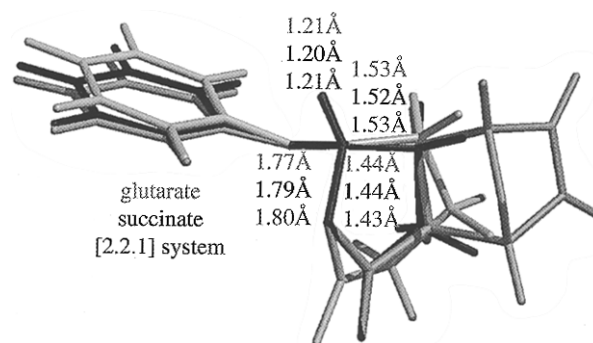
TS for reaction **I** (O2–C5–O10) is slightly smaller (113.7°). This difference is most likely attributed to glutarate forming a six-membered anhydride ring while both succinate and 3,6-endoxo-Δ^4-tetrahydrophthalate form five-membered anhydride rings. As both the distances and the angles are concerned, the transition states formed for reactions of **I**, **II**, and **III** are essentially identical. Phenoxide departure is concerted with carboxylate attack for reactions of **I** and **II**, and departure of phenoxide is early for reactions of **I**, **II**, and **III**.

Vibrational Frequency Changes upon Reaching the TS. In the arguments of entropy as being the driving force for enzyme catalysis and intramolecular reactions, it has been proposed that the restriction or dampening of low frequency vibrations allows the attainment of more favorable entropy of activation.[2] However, little has been done to calculate and verify these speculations. One might feel comfortable believing that when two molecules, each having three degrees of translational motion and three degrees of rotational motion, meet and form a complex, the complex will have converted the six extra degrees of motions to new vibrations at the interface of the two molecules, increasing the total number of vibrations. Why then would moving from the complex to the transition state dampen or restrict the existing vibrations? This concept seems to be widely accepted. Figure 3 is a graphical representation of the calculated frequencies pertinent to the reactions of **I**, **II**, and **III**. The frequencies of interest are the frequencies for the IIMC (and tetrahedral intermediate) compared to the corresponding TS. The total number of frequencies does not change in going from the IIMC (or TI) to the TS for each ester (Table 6). Knowing that the lower frequencies contribute more to the entropy of the structures and following the Page and Jencks criteria[2] of frequencies lower than 1000 cm^{-1}, the number of lower frequencies remains constant from the IIMC or TI to the

transition state (the imaginary frequency characterizes the transition state). The other implication from the Page and Jencks speculations are that the larger the experimental rates, the more frequencies will have to be dampened out. Since we cannot compare the absolute number of frequencies between compounds, we have taken the ratio between the number of low frequencies (below 1000 cm^{-1}) and the total number of frequencies. The ratios of the IIMCs (TI) or the TS low frequencies to the total number of frequencies for the anhydride formation of **I**, **II**, and **III** are 0.49, 0.51, and 0.55, respectively. The trends of these ratios is that the faster the reaction, the more low frequency vibrations. So, whether the frequencies are compared within a monophenyl ester or the ratio of low frequencies to total frequencies is compared between esters, we do not observe any dampening or restriction or freezing out of the low frequency vibrations.

Reactant Side Structures. The number of transition states in the reactions of **II** and **III** are limited by the rigidity of their systems. In the case of **II**, there is only one possible transition state because the five-membered anhydride is planar. In the case of **III**, the two possible transition states have been found. However, in the case of **I**, the flexibility of the six-membered anhydride that is being formed may allow more than one possible transition state structure. Using an IRC calculation from the TS to the reactant side, structures were located along the slope of the reaction coordinate between the IIMC and the TS. A large conformational change is observed in going from the IIMC to the TS in the reaction of **I**. Figure 6a shows that the IIMC has a puckered six-membered ring with the C6 methylene puckered toward the leaving phenoxide and a C5−C9−C6−C3 torsion angle of −88.5°. As the reaction proceeds toward the TS, the C6 methylene starts puckering away from the leaving group (Figure 6b). At this point, the methylene hydrogens of C9 and C6 are nearly eclipsed, and the C5−C9−C6−C3 torsion angle is −24.1°. Figure 6c is the transition state where C6 is puckered away from the leaving group, and the C5−C9−C6−C3 torsion angle is 20.4°. This conformational change is caused by the electrostatic attraction between the acidic α-carbon (C9 and C3) hydrogens and the developing partial negative charge on the leaving phenolate oxygen. The distances between the C9 and C3 hydrogens to the phenolate oxygen are 2.41 and 2.40 Å, respectively. Because of this oxygen−hydrogen interaction, this transition state would be stablized and is most likely the lowest energy transition state. In the IIMC, the oxygen of the phenolate is less negative than when in the transition state; thus, little stabilization would be gained from interacting with the C9 and C3 hydrogens. If there is an IIMC where C6 is puckered away from the leaving group, a smaller conformational change would be required to enter the TS. Thus, most likely, the calculated TS is the same TS for other possible IIMCs.

In our previous MM3(92) studies of the ground states of the monoesters of Table 1,[3] those conformations in which the carboxylate oxygen is in the correct alignment with the ester carbonyl carbon for nucleophilic attack were identified (Chart 1) and characterized. They have been referred to as **N**ear **A**ttack **C**onformations (NACs). The distance between carboxylate oxygen and ester carbonyl carbon for the NACs of **I** (3.20 Å), **II** (3.08 Å), and **III** (2.93 Å) and other monoesters of Table 1 is ∼3 Å.[3] For **I** and **II** of this current study, the nearest local minimum to the transition state on the reactant side is the intramolecular ion−molecule complex (IIMC). These IIMCs have the geometrical characteristics of a NAC but differ by the distances for the carboxylate oxygen to ester carbonyl carbon, 2.71 and 2.69 Å for reactions **I** and **II**, respectively. These
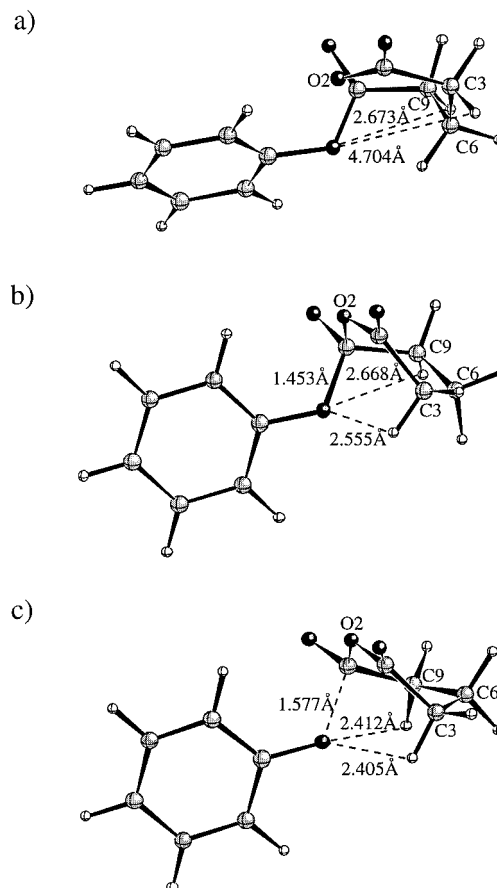

Figure 6. (a) The optimized IIMC of **I** where the C6 methylene is puckered toward the leaving phenoxide. The torsion angle of C5−C9−C6−C3 is −88.5°. (b) A structure along the upward slope between the IIMC and the TS where the C6 methylene is changing to pucker away from the leaving phenoxide. The torsion angle of C5−C9−C6−C3 is −24.1°. (c) The optimized TS where the C6 methylene is puckered away from the leaving group. The torsion angle of C5−C9−C6−C3 is 20.4°.

distances are ∼0.4 Å shorter than those found in the NACs. Also, there is the presence of a hydrogen bond between a carboxylate oxygen and an *ortho*-hydrogen of the esterified phenol. Thus, if NAC and IIMC were placed along the reaction coordinate, the IIMC would be further along the reaction toward the TS. In the case of **III**, the nearest local minimum to the TS is a tetrahedral intermediate.

In examination of the energy difference between the transition state and the intramolecular ion−molecule complex (IIMC) or tetrahedral intermediate, one should note both ΔH_R^{298} and ΔE_R (Table 8) decrease in the order of **I** > **II** > **III**. On the other hand, (Figure 7) $T\Delta S_R^{298}$ is rather invariant with change of ester. The free energies for the reactions of **I** and **II** are also listed in Table 8. The experimental $\Delta\Delta G^{\ddagger}$ for the reactions of **I**, **II**, and **III** are as follows: between **I** and **II** is 3.27 kcal/mol; between **II** and **III** is 3.28 kcal/mol.[16] Though the computed $\Delta\Delta H_R^{298}$ and $\Delta\Delta G_R^{298}$ between **I** and **II** are comparable to the experimental $\Delta\Delta G^{\ddagger}$, the difference between $\Delta\Delta H_R^{298}$ ($\Delta\Delta G_R^{298}$) and $\Delta\Delta G^{\ddagger}$ in comparing **II** and **III** is large. Though the experimental solution values of $\Delta G^{\ddagger}$ do not correlate directly with the gas phase ΔG_R^{298}, trends are comparable. One must keep in mind that in the gas phase calculations, the lowest ground state is the IIMC. The carboxylate oxygen to carbonyl carbon distances in the IIMC geometries arising from **I** (2.71 Å) and **II** (2.69 Å) and the carboxylate oxygen to carbonyl

(16) Bruice, T. C.; Pandit, U. K. *J. Am. Chem. Soc.* **1960**, *82*, 5858.
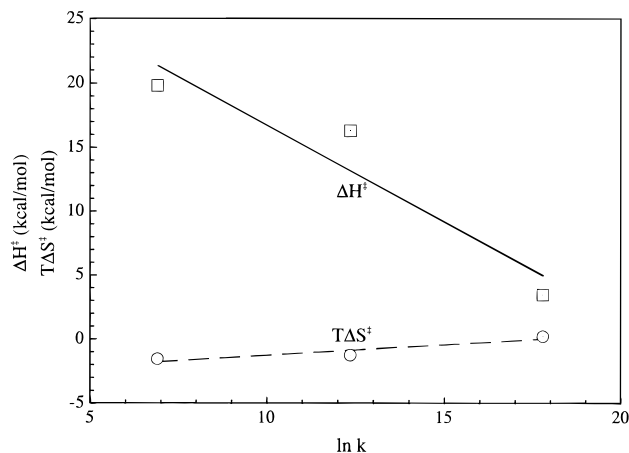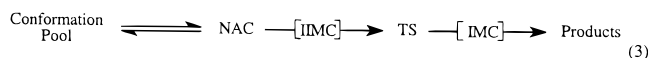
Figure 7. A plot of the *ab initio* calculated ΔH_R^{298} and $T\Delta S_R^{298}$ vs the log of the relative rate constant (k_r).

Table 8. Energy Differences between the Transition State and Intramolecular Ion−Molecule Complex (IIMC) or Tetrahedral Intermediate (TI) (kcal/mol)

ester	$\Delta E_R{}^a$	$\Delta H_R^{298\,a}$	$\Delta S_R^{298\,a}$	$\Delta G_R^{298\,a}$
I	20.96	19.80	−5.26	21.37
II	17.64	16.28	−4.25	17.55
III[b]	4.28	3.43	0.63	3.24

a The subscript R refers to the reaction side energy differences. *b* Ester **III** has a TI not an IIMC.

carbon bond length in the TI from **III** (1.55 Å) decrease in a similar trend as the decreasing values of ΔE_R (Table 8). Simply put, the carboxylate oxygen and carbonyl carbon of **III** is constrained to be closer than **I** or **II** because of the caged structure. This restrictive cage facilitates the formation of a tetrahedral intermediate in the gas phase. However, in the determination of the experimental $\Delta G^{\ddagger}$, the ground state is a collection of conformations mostly in the low energy extended state. The calculations which include solvation effects present a more correlated picture (*vida infra*). Reaction coordinates computed by *ab initio* methods in solution show the extended conformation to be of energy below the transition state and IIMC. So, along the reaction path from extended structure to TS, the IIMC would be a necessary structure. Combining the results of the ground state studies using molecular mechanics[3] and the reaction coordinate studies by *ab initio* methods, we arrive at eq 3 and the cartoon reaction coordinate of Figure 8

$$\text{Conformation Pool} \rightleftharpoons \text{NAC} \longrightarrow [\text{IIMC}] \rightarrow \text{TS} \longrightarrow [\text{IMC}] \rightarrow \text{Products} \tag{3}$$

for reactions in polar solvents. Considering Figure 8, for a given ester the energy difference between the (MM3 derived) NAC (Figure 1) and (*ab initio* derived) IIMC (or TI) is unknown such that the energy difference between NAC and TS cannot be calculated.

In fashioning a cartoon showing the reaction coordinates for a series of esters becoming anhydrides plus phenolate, we will start with the transition state energies normalized to a constant value (Figure 8). This has been done to emphasize (i) the portions of the transition state structures which are involved in bond making and breaking (Chart 7) and are structurally superimposable−identical bond lengths and angles (Figure 5) and (ii) the loop portion of the structure of Chart 7 which depicts the essentially strain-free five- and six-membered rings. The actual transition state energies are, of course, quite different because the empirical formulae of the three transition states are different. Normalization of the transtion state energies to a
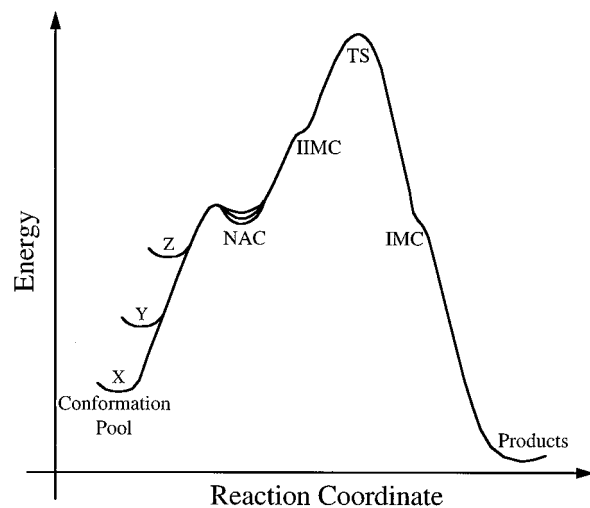

Figure 8. Reaction coordinate cartoon for the intramolecular reactions in polar solvent for esters X, Y, Z. The conformation pool is the equilibrium of conformational local minimas, including the global minimum. The NAC is the near attack conformation. The IIMC is the intramolecular ion−molecule complex, which corresponds to the gas phase nearest local minimum on the reactant side to the transition state (TS). The IMC is the ion−molecule complex, which is the nearest local minimum on the product side to the transtion state. Products are the anhydride and the phenoxide. The marked characteristics of the cartoon are the superimposable transition states structures and the common characteristics of NACs.
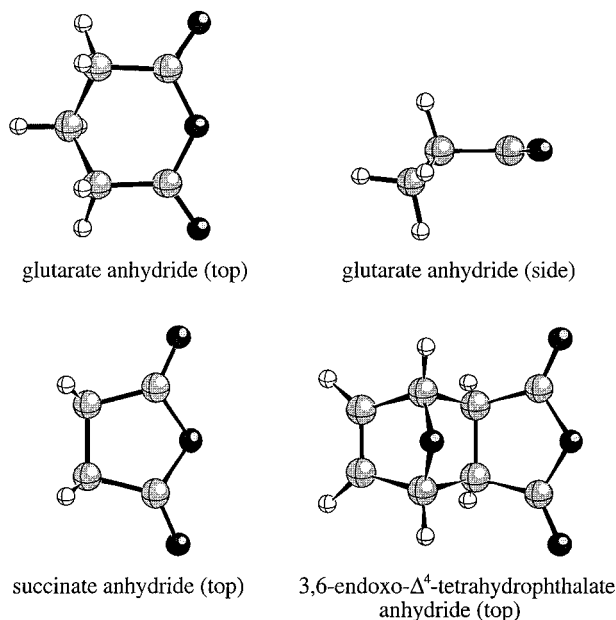
Chart 7
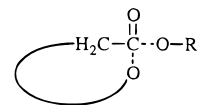
common value allows one to observe (Figure 8) the differences in the average Boltzmann energies of the "Conformation Pool" of reactants. The mole fraction of NACs in the Conformation Pool would then dictate the changes in rate constants in going from esters X to Y to Z.

Identification of NACs for a particular ester is not synonymous with identification of the transition states for reaction (i.e., each NAC does not give rise to one particular TS). As an example, there are five identified NACs among the eight conformations of **III** (Figure 1) but only two TSs (Chart 5). TS2 is less stable than TS1 by ∼9 kcal/mol. Thus, the important pathway involves five NACs to TS1. For ester **II**, there are six NACs among 108 ground state conformations (Figure 1). One NAC is of much higher energy than the others, but there is only one TS. Seemingly, different NACs can converge along the free energy landscape to a common TS, possibly passing through the same IIMC.

Product Side Structures. We now turn our attention to the product side which involves TS → IMC → products. In the gas phase, the products of each of **I**, **II**, and **III** are higher in energy than the transition state and the product side ion−molecule complex (Figure 4). The energy for the products is the sum of the energies for the anhydride and phenoxide. The five-membered anhydrides formed in the reactions of **II** and **III** are planar (Chart 8). The two sp^2 carbons limit the flexibility in puckering. The six-membered anhydride formed from **I** is not so limited such that two energetically equivalent conformations, puckered up and puckered down, are formed (Chart 8). Table 9 reports the RHF, enthalpic, entropic, and free energies of the ion−molecule complex relative to the transition state. When comparing the energies of IIMCs (or TI) to IMCs, the reaction of **I** (3.39 kcal/mol) and **II** (6.03 kcal/mol) are

Chart 8

glutarate anhydride (top)   glutarate anhydride (side)

succinate anhydride (top)   3,6-endoxo-Δ^4-tetrahydrophthalate
                                              anhydride (top)

Table 9. Energy Differences between the Transition State and the Product Side Ion−Molecule Complex (IMC) (kcal/mol)

ester	$\Delta E_P{}^a$	$\Delta H_P{}^{298\ a}$	$\Delta S_P{}^{298\ a}$	$\Delta G_P{}^{298\ a}$
I	16.57	16.03	−18.33	21.49
II	11.61	10.90	−14.04	15.09
III	12.66	11.90	−13.36	15.88

^{a} The subscript P refers to the product side energy differences.

endothermic, while the reaction of **III** is highly exothermic (−7.38 kcal/mol, Figure 4). Because these calculations are of unsubstituted phenyl esters, we would expect that the reactions of **I** and **II** would not necessarily be thermodynamically favorable. However, we might anticipate that the reaction of **III** would be thermodynamically favorable. This is consistent with the experimental kinetics studies[4] where the reactions of both the unsubstituted monophenyl esters of glutarate and succinate were too slow to be measured. However, when the leaving group is p-BrC$_6$H$_4$O$^−$, the reactions are accelerated to a measurable level. With the p-BrC$_6$H$_4$O$^−$ ester of 3,6-endoxo-Δ^4-tetrahydrophthalate, the reactions were so rapid that they could not be followed. The p-methoxyphenyl ester was used to decrease the rates to manageable levels. The reaction rate of the p-methoxyphenyl ester of 3,6-endoxo-Δ^4-tetrahydrophthalate was correlated with the a p-bromophenyl ester of glutarate and succinate using σ-ρ relationship. In terms of the change in free energy (Table 9), the trend is similar to that of the ΔE. Again, the reaction of succinate is endothermic, and 3,6-endoxo-Δ^4-tetrahydrophthalate is exothermic. On the other hand, glutarate seemingly will have a thermodynamic equilibrium between the IIMC and the IMC with a very large kinetic barrier. The geometry of the IMC with a six-membered anhydride complexed to the phenoxide is noticeably different from the five-membered IMCs. The distance between the anhydride carbon to the phenoxide oxygen is greater for glutaric anhydride IMC (4.06 Å) than for either the succinic anhydride IMC (3.02 Å) or the 3,6-endoxo-Δ^4-tetrahydrophthalate anhydride IMC (3.00 Å).

Solvation and Electron Correlation Calculations. The gas phase HF/6-31+G(d) calculations resulted in the reaction coordinates shown in Figure 4. Since this is an ionic reaction, we expect that solvation may have a large effect on the calculated reaction barrier. To estimate the solvation effects

on the activation barriers, single point calculations using different solvation methods with a dielectric constant of water were performed on the optimized gas phase HF/6-31+G(d) structures formed in the reactions of **I**, **II**, and **III**. From Table 7, the HF solvation model (HF/6-31+G(d)/SCRF-SCIPCM) produced, as expected, larger barriers than the gas phase barriers. Also, as expected, the extended structures of **I** and **II** were more stable in the solvation calculations than their respective IIMCs.[17] Single point calculations were also performed using a method to include the electron correlation in both gas phase and solvation, B3LYP/6-31+G(d) and B3LYP/6-31+G(d)/SCRF-SCIPCM methods, respectively. Here, the gas phase B3LYP/6-31+G(d) calculations estimate very low barriers of activation where the barrier from the TI to the TS in the reaction of **III** is only 1.92 kcal/mol (Table 7). Nonetheless, the solvation estimation with an electron correlation method (B3LYP/6-31+G(d)/SCRF-SCIPCM) seems to be in the best agreement with energy barriers calculated from experimental reaction rates. These experimental barriers are (i) 23.47 kcal/mol for the reaction of **I**, (ii) 20.19 kcal/mol for the reaction of **II**, and (iii) 16.92 kcal/mol for the reaction of **III**,[16] which are the sum of $\Delta H^{\ddagger}$ and $\Delta S^{\ddagger}$. The calculated solvation barriers are $\Delta E^{\ddagger}$ (which is $\sim\Delta H^{\ddagger}$, Table 7), and thus, it is not surprising that the calculated solvation barriers are slightly smaller than the experimental barriers. Also, the barriers for reactions of **I** and **II** are calculated from their IIMCs. Because the single point calculations for the extended conformations were unable to converge, barriers from the extended structures for reaction **I** and **II** are not available. But, similar to the HF/6-31+G(d) solvation calculations, the extended structure energies from the B3LYP/6-31+G(d) solvation method would be expected to be lower in energy than the IIMCs. Presumably, when comparing the activation barriers from the IIMC with those from the extended structures, the energy difference is attributed to the energy from the extended structure to the IIMCs.

Conclusions

In previous investigations[3] there were determined for each ester (Table 1) (i) the rate constants for intramolecular displacement of phenoxide to form anhydride (effective molarities vary between 10^3 and 10^8 M) and (ii) by use of molecular mechanics and statistical mechanics, the distribution of ester ground states and the energies, enthalpies, and entropies of each conformer (Figure 1). It could be shown that $\Delta G^{\ddagger}$ was linearly related (slope $\sim$ 1.0) to the log of the mole fraction (**P**) of conformations present as Near Attack Conformations (NACs). Further, log **P** was shown to be dependent upon the enthalpy of NAC formation ($\Delta H°$) rather than the entropy ($\Delta S°$) (Figure 2). The conclusion was reached that the stability of NAC conformations determine the rate constants, and this stability is enthalpically controlled. The present study also supports this position.

The monophenyl esters of glutaric (**I**), succinic (**II**), and 3,6-endoxo-Δ^4-tetrahydrophthalic (**III**) acids are representative of the esters of Table 1. *Ab initio* gas phase calculations at the RHF/6-31+G(d) level were employed to locate the transition states and, by the intrinsic reaction coordinate calculations, identify the immediate reactant {intramolecular ion−molecule

---

(17) Because AM1/SM2.1 was parameterized to reproduce the experimental solvation free energies, AM1/SM2.1 solvation calculations were also performed on the gas phase HF/6-31+G(d) geometries. The calculated free energies of solvation were added to the gas phase HF/6-31+G(d) electronic energy. These AM1/SM2.1 solvated energies show that the IIMC of **I** is slightly lower in energy than its extended structure (Table 7). For **II**, the IIMC is $\sim$3 kcal/mol lower in energy than its extended structure. Because we anticipated that experimentally in water the extended structure should be lower in energy than the IIMC, the AM1/SM2.1 solvation estimation does not seem to be a good method for this system.

complex (IIMC) and tetrahedral intermediate (TI)} and product {ion−molecule complex of anhydride and phenoxide (IMC)} structures and their energies. The transition states for the formation of anhydrides from **I**, **II**, and **III**, which involve departure of the leaving phenoxide, are essentially identical when comparing bond distances and bond angles for the nucleophilic oxygen to carbonyl carbon and for the carbonyl carbon to leaving phenoxide oxygen, carbonyl oxygen, and α-carbon (Figure 5). Thus, though the experimental rate constants increase by ∼230-fold on going from **I** to **II** and from **II** to **III**, the transition state structures for the three reactions are superimposable. Freezing out of low frequency vibrations in the transition states do not play a role in the increase in rates. Aside from the conversion of a single real frequency to an imaginary one (Figure 3), the frequency calculations do not reveal the disappearance of any low frequency vibrations upon entering the transition states. Therefore, changes in rate constants must be due to ground state phenomena (Figure 8), and from the previous MM study, the difference in rate constants can be related to the ease by which an extended ground state can become a NAC for any given ester (Figure 1).